Chapter IV Thermo-Mechanical Analysis

4.1 Outline

In this chapter, the FEM thermo-mechanical modeling results of the wire bond module and the MPIPPS are presented first. A fatigue life prediction on the MPIPPS module solder joints is then performed. The wire bond module reliability is finally discussed.

4.2 Thermo-Mechanical Characteristics of the Wire Bond Module vs. the MPIPPS Module

4.2.1 The Wire Bond Model

The wire bond modeling results show no observable change in stress and strain in the wire bonds during the 15-minute holding period. This is because that there are no time-dependent material characteristics in the wire bonds.

Figure IV-1 shows the critical locations in wire bond model after an overall review of the stress and strain condition.

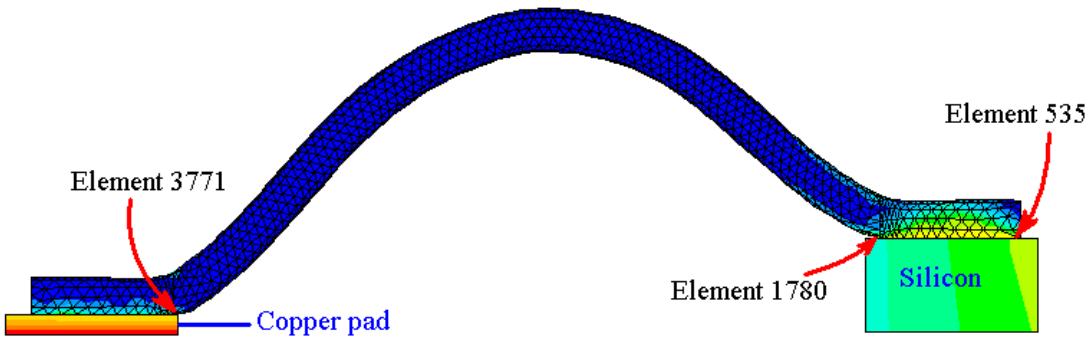

Figure IV-1 Critical Locations in the Wire Bond Model

Figure IV-2 and Figure IV-3 show the Von Mises stress distribution after three temperature cycles and power cycles, respectively.

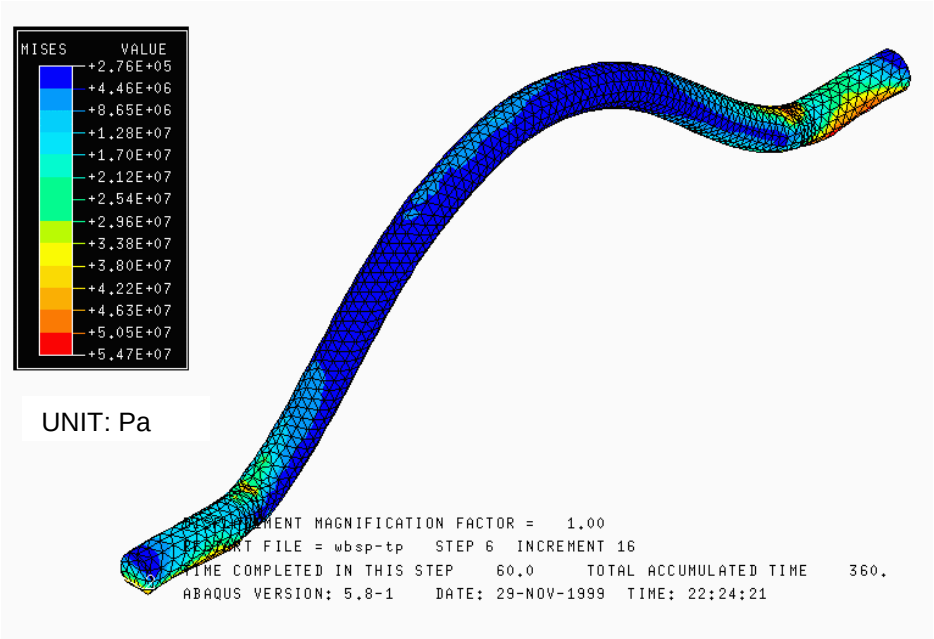

Figure IV-2 Von Mises Contour of the Wire Bond under Temperature Cycling, at the End of the 3rd Cooling Stage

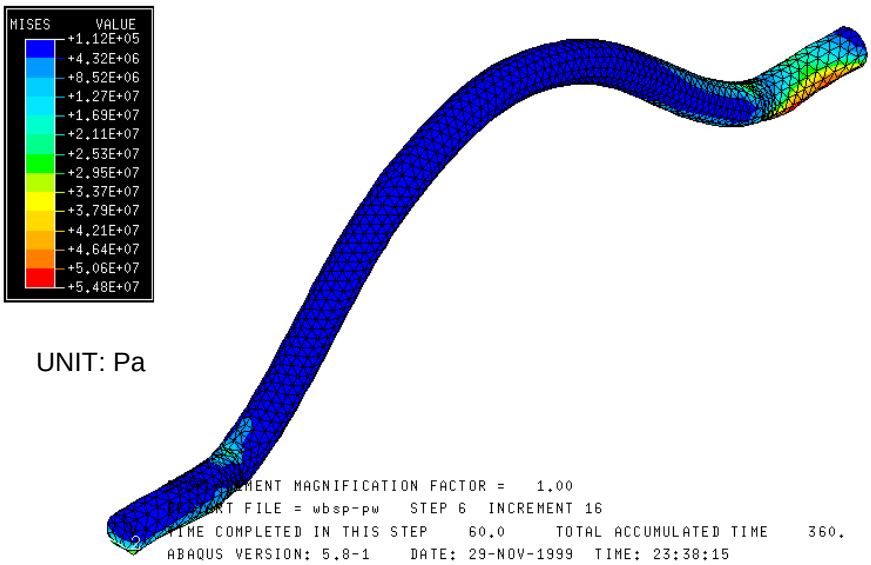

Figure IV-3 Von Mises Contour of the Wire Bond under Power Cycling, at the end of the 3rd Cooling Stage

Under temperature cycling conditions, both ends of the aluminum wire show some stress concentration in the regions where they bond to the pad and device. While under power cycling condition, the stress levels are a little bit higher at the device end of the wire, the wire-pad area and the bow-shaped area show up to two times less in stress, compared with those under temperature cycling. The reason for this difference is that under temperature cycling conditions, the model is uniformly heated from the cold stage to the hot stage, back and forth. The stress conditions are similar for the two ends of the bonding wires. While in power cycling, the device end of the wire could be 80^{o}C hotter than the other end; therefore, due to the large CTE mismatch between aluminum and silicon ($\Delta\alpha = 19 \times 10^{-6}$ /K), stresses build up in this region.

The equivalent plastic strain (PEEQ) is used here to evaluate the yield condition of the wire bonds. In an isotropic hardening plasticity theory, for most materials the PEEQ is defined as $\sqrt{\frac{2}{3} d\varepsilon^{pl} : d\varepsilon^{pl}}$, and is the total accumulation of plastic strain to define the yield surface size.[1]

The following figures show the similar PEEQ developed in the bonding wire at the wire-device interface during temperature (Figure IV-4) and power cycling (Figure IV-5). Two regions have been identified as critical, elements 535 and 1780, due to their relatively large plastic deformation.

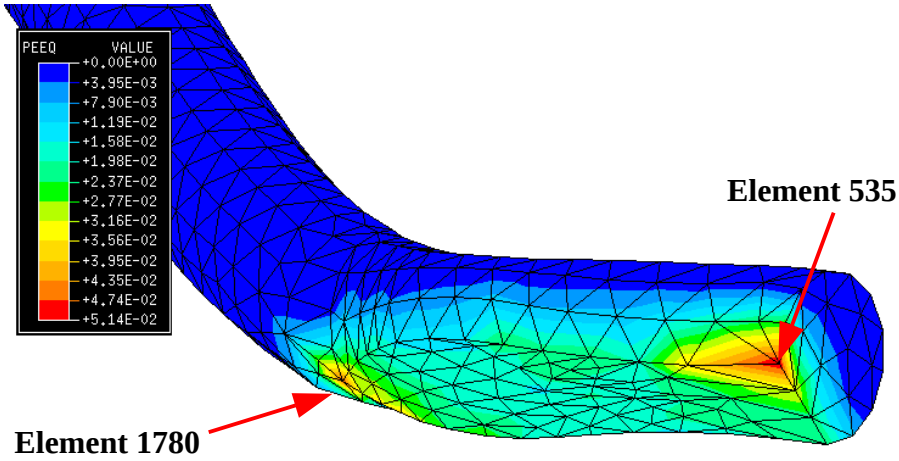

Figure IV-4 PEEQ Contour for Device-side Wire Bond, Temperature Cycling, At the End of the 3rd Cooling Stage

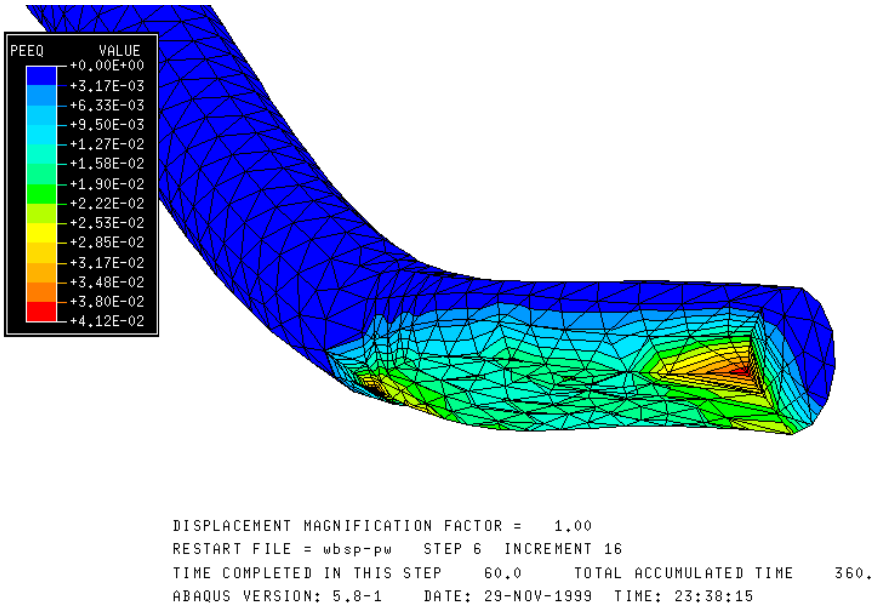

Figure IV-5 PEEQ Contour for Device-side Wire Bond, Power Cycling, At the End of the 3rd Cooling Stage

Figure IV-6 clearly shows the plastic strain developed in the bonding wire at the wire-pad interface during temperature cycling. On the other hand, there is almost no plastic deformation in the same region during power cycling.

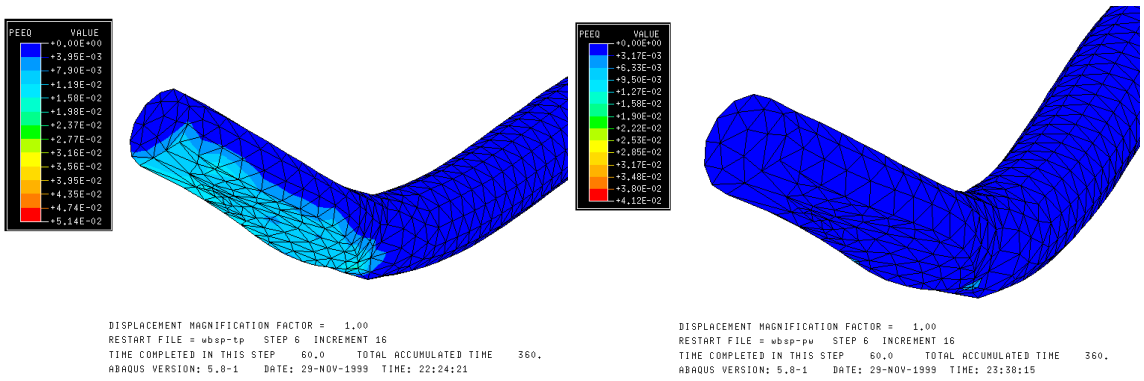

Figure IV-6 PEEQ Contour for Pad-side Wire Bond, Temperature Cycling (left), Power Cycling (right), At the End of the 3rd Cooling Stage

Figure IV-7 shows the similarity of the inelastic strain histories of element 535 in both cycling conditions.

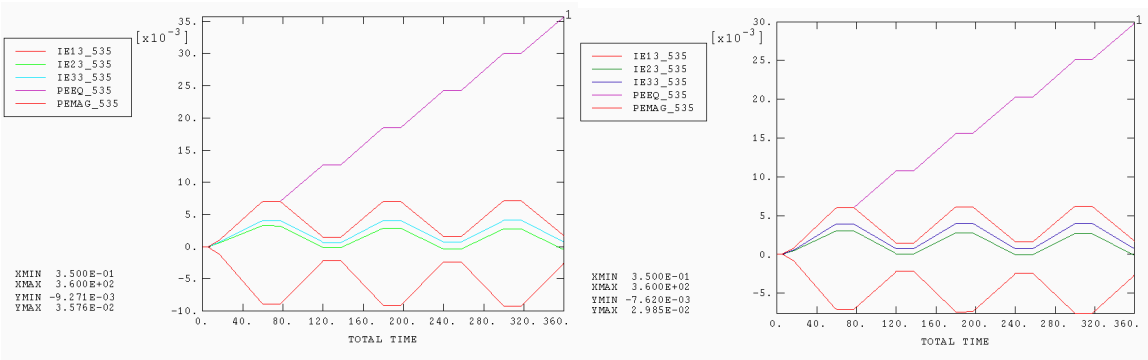

Figure IV-7 Inelastic Strain Histories for Element 535 at Temperature Cycling (left) and Power Cycling (right)

As stated earlier in this chapter, due to the fact that there are no creep characteristics present in the aluminum wires, even if considering the creep of the solder material used for die attachment, the stress and strain conditions have no observable change during several runs of sample problems. Therefore, only the heating and cooling (both at a rate of 125 ^{o}C per minute) stages are modeled and there is no need for 15 minutes' holding

period, as was used in the MPIPPS models. Also, the inelastic behavior of the bonding wires can be represented only by the plastic component PEEQ, since there is no other inelastic response.

Figure IV-8 shows the similarity in the inelastic strain histories of element 535 in both cycling conditions.

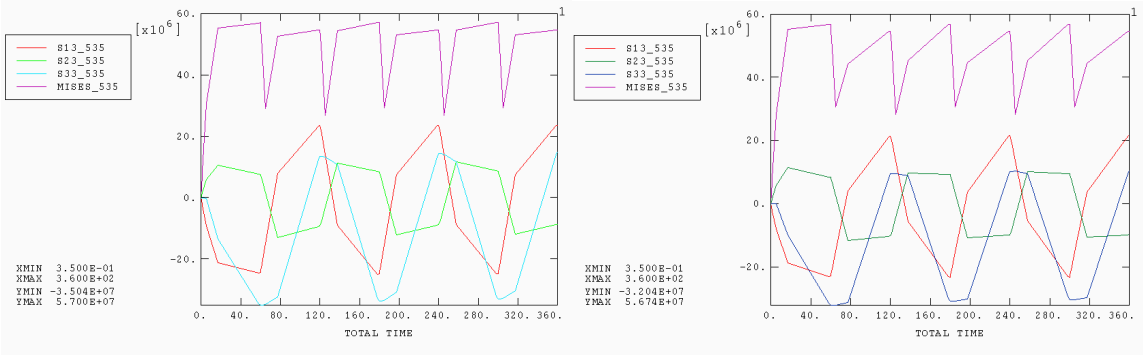

Figure IV-8 Stress Histories for Element 535 at Temperature Cycling (left) and Power Cycling (right)

Figure IV-9, on the other hand, shows different strain conditions at element 1780 that occur due to different thermal loadings. Under temperature cycling, there is relatively larger plastic deformation at this location, and therefore relatively smaller stresses due to the relaxation.

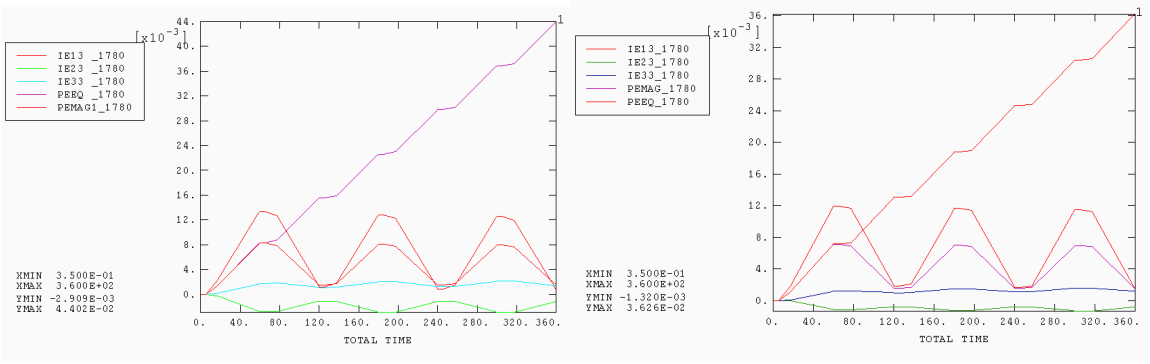

Figure IV-9 Inelastic Strain Histories for Element 1780 at Temperature Cycling (left) and Power Cycling (right)

Because element 1780 is right located at the structural singularity position, a stress curve for z-direction is not available from the FEM results file. Only the contour plot of the z-direction stress at the end of the 3rd cooling stage is shown (Figure IV-10, left and right). Both figures show a tensile stress at the wire-device interface and at the same time, a compressive stress of similar magnitude just above the interface in the aluminum wire. A better mesh should be able to avoid this problem and construct the geometry just like the real interface.

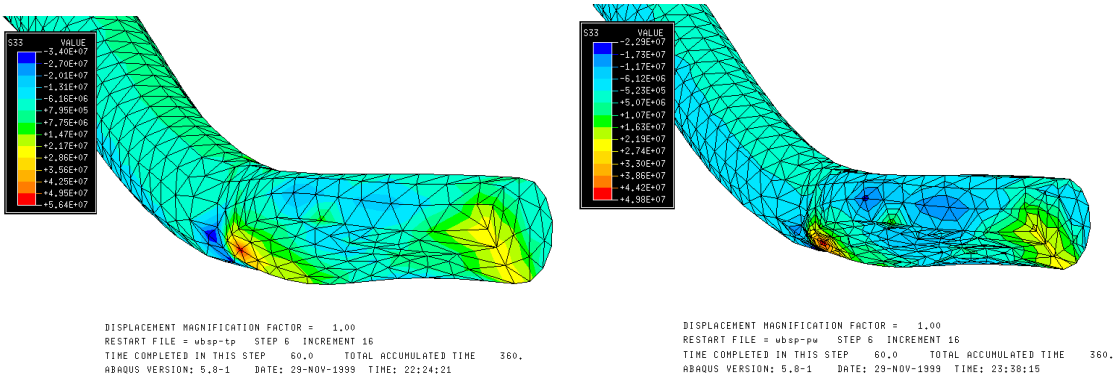

Figure IV-10 Normal Stress σ_3 Contour in Device-side Wire Bond Under Temperature Cycling (left) and Power Cycling (right)

The schematics of the deformed shape of the wire bond in both cycling conditions (the 3rd heating stage for both) are shown in Figure IV-11 and Figure IV-12 (drawing not to scale). The red mesh represents the original undeformed model. Compared with the results of power cycling, temperature cycling proves to be more detrimental to the wire bond module because the wire bows more and thus is bent up to a non-negligible angle at the joint between wire and device. Note that at the location where the element 1780 lies, a crack is easily developed during the cycling conditions. This situation worsens over time, and failure of the module due to debonding is anticipated. The range of maximum z-direction displacement (in some references out-of-plane displacement) is about 10-16 microns.

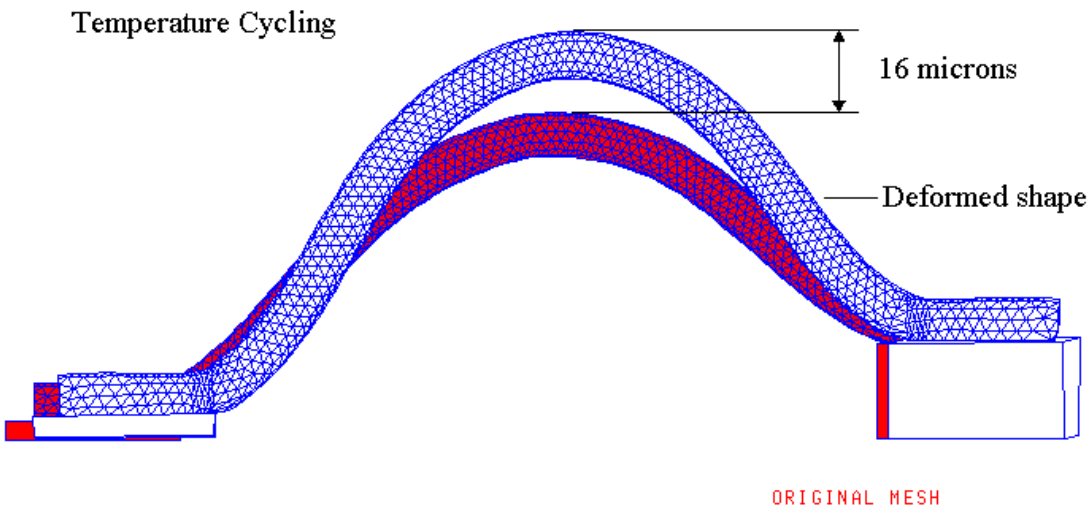

Figure IV-11 Deformation Plot of the Wire Bond under Temperature Cycling, At the end of the 3rd Heating Stage (Drawing Not to Scale)

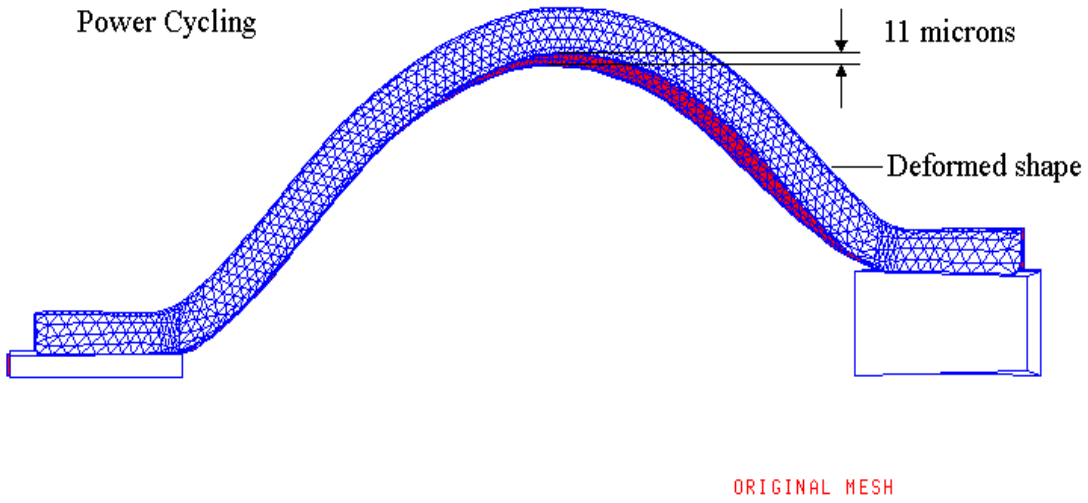

Figure IV-12 Deformation Plot of Wire Bond under Power Cycling, At the end of the 3rd Heating Stage (Drawing Not to Scale)

Temperature cycling creates higher mechanical stresses on both ends of wire bonds while power cycling only threatens the device side. Under a similar maximum junction temperature, temperature cycling causes more damage to the module.

4.2.2 MPIPPS Model

An exaggerated deformation plot of the solder joints between the copper post and the top DBC substrate is shown in Figure IV-13. This deformation occurs at the end of the 3rd heating cycle in temperature cycling. Apparently the solder expands much more than the post and the DBC. An overall review of the stress-strain, as well as deformation status of the model during temperature cycling and power cycling, helps identify the weak locations: they are at elements 7194, 7204 and 6469, as shown in Figure IV-13

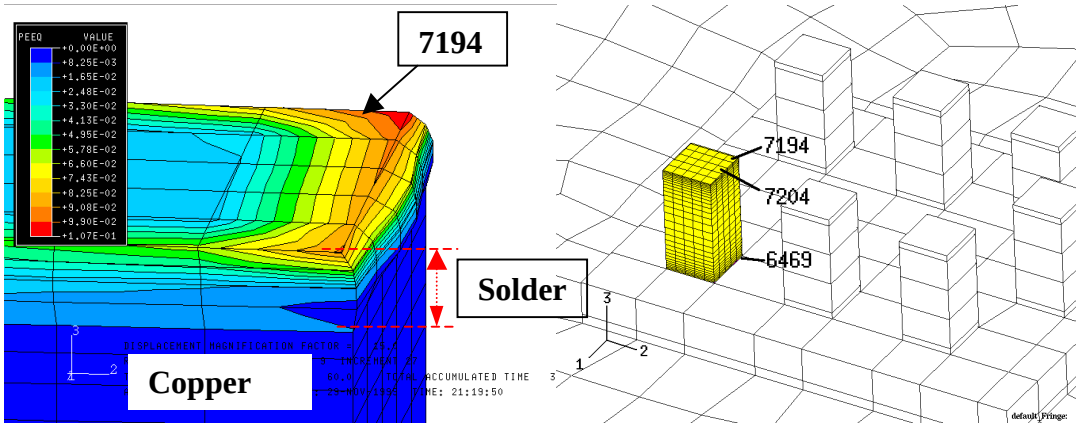

Figure IV-13 Determination of Critical Locations in MPIPPS Model

The total strain is composed of elastic strain, thermal strain, plastic strain and creep strain. The modeling results (Figure IV-14 shows strain curves of element 7204 as an example) have shown a very small elastic strain and thermal strain in the solder material.

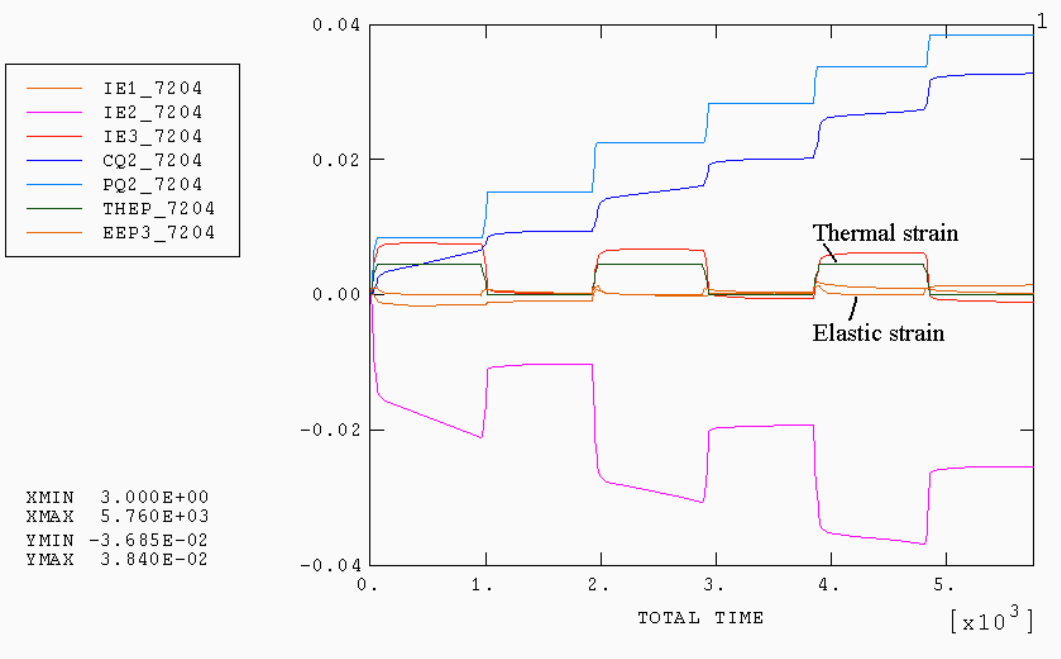

Figure IV-14 Total Strain Components for Element 7204 under Temperature Cycling

The inelastic strain, which is composed of plastic strain and creep strain, constitute the greatest strain. After initial review of the modeling results, we can conclude that the plastic deformation and creep occur simultaneously in solder material in the MPIPPS model. In this thesis, a constitutive theory based on the classical creep and plasticity concept is used to model temperature-dependent, visco-plastic deformation behavior of the solders, as developed by Hong and Burrell.[2] The visco-plastic strain IEEQ (equivalent inelastic strain) is defined as the sum of the equivalent creep strain CEEQ and the equivalent plastic strain PEEQ.[3] As mentioned earlier in this chapter, PEEQ is the total accumulation of plastic strain to define the yield surface size.[1] And the CEEQ is defined by the same formula given above for PEEQ, but applied to the creep strains.[1]

There is a potential problem, however, in using the elastic and pure plastic model for eutectic solder, which researchers have used in some situations. Figure IV-15 shows a comparison of the PEEQ of element 7204 in MPIPPS models using different plastic models of eutectic solder (under temperature cycling). The model that assumes elastic and pure plastic shows much larger plastic deformation than does the model of elastic and kinematic hardening after material's yielding.

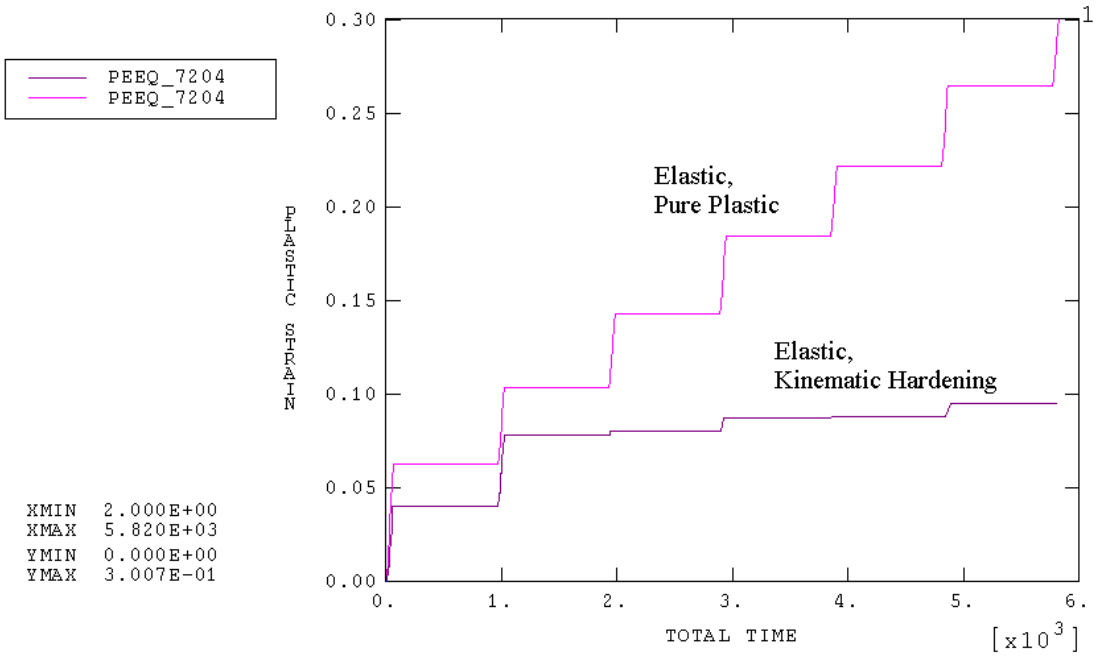

Figure IV-15 Comparison Between Pure Plasticity and Kinematic Hardening Plasticity for Modeling Eutectic Solder Material

The reason for that is that ABAQUS (as well as MSC/PATRAN ADVANCED FEA) calculates the elastic behavior first, then the creep behavior, and after that the plastic behavior.[4] Since the thermo-mechanical problem is solved by a sequential nonlinear static stress analysis, multiple increments are needed, with each incremental based on the previous increment. Substantial errors in creep analysis could occur if the plastic strain is too large in each increment. In order to minimize the plastic strain increments, small time increments need to be used. On the other hand, the use of a kinematic hardening plastic model for solder, which more closely models real solder behavior, also helps minimize the plastic strain increment, and thus gives better results.

Figure IV-16 shows the average equivalent creep and equivalent plastic strain in elements 7194, 7204 and 6469 in temperature cycling. Figure IV-17, Figure IV-18 and Figure IV-19 show the Von Mises stress, the CEEQ and the PEEQ, respectively (viewing from [1,1,1]). After three cycles, creep deformation dominates the inelastic behavior of solder. The worst deformation occurs in element 7194, where the solder joins the top DBC. Shown in the elastic, kinematic hardening model curve in Figure IV-16 (also

pointed out by B. Hong[3]), the eutectic solder displays a relatively weak resistance to the high-temperature, low-stress creep, and a strong resistance to high-temperature plastic deformation. In the 2nd and more so in the 3rd heating stage, the PEEQ has a very small increment, while at the same time the CEEQ increase dominates that of the IEEQ. This is not observed in the elastic, pure plastic model. Therefore, the use of a kinematic hardening model is a better choice in terms of accuracy.

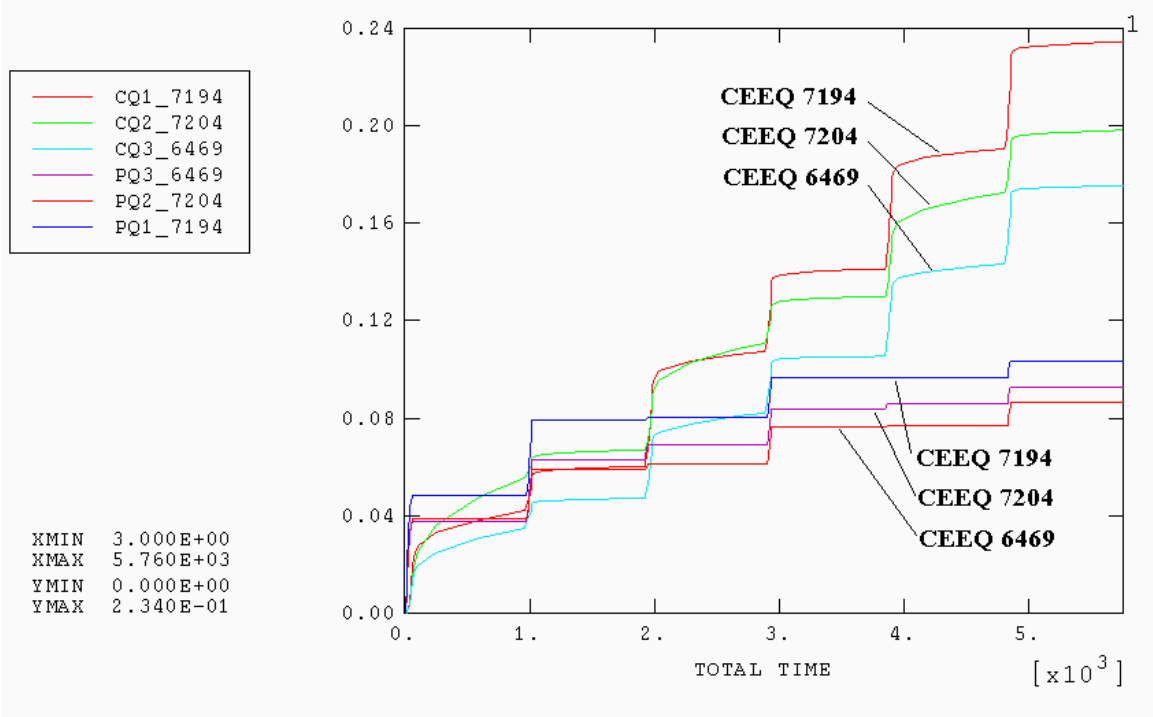

Figure IV-16 Average CEEQ and PEEQ in Element 7194, 7204 and 6469 under Temperature Cycling

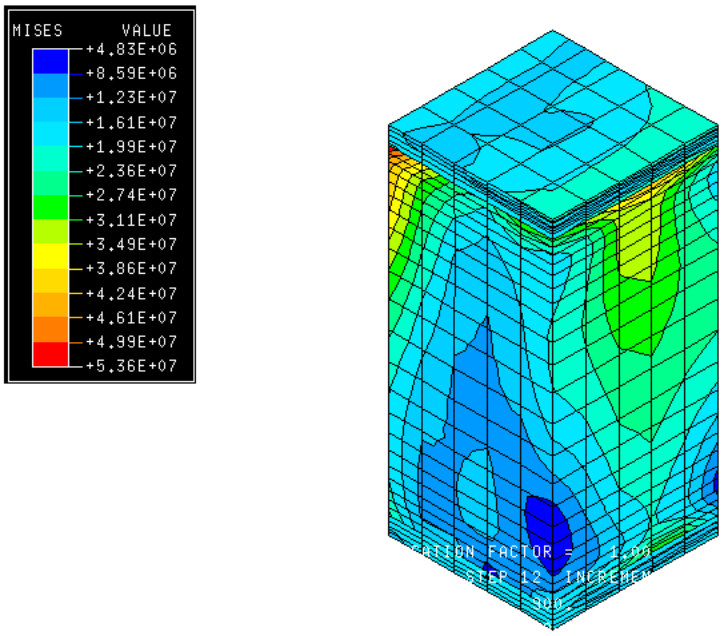

Figure IV-17 Von Mises Stress Contour under Temperature Cycling

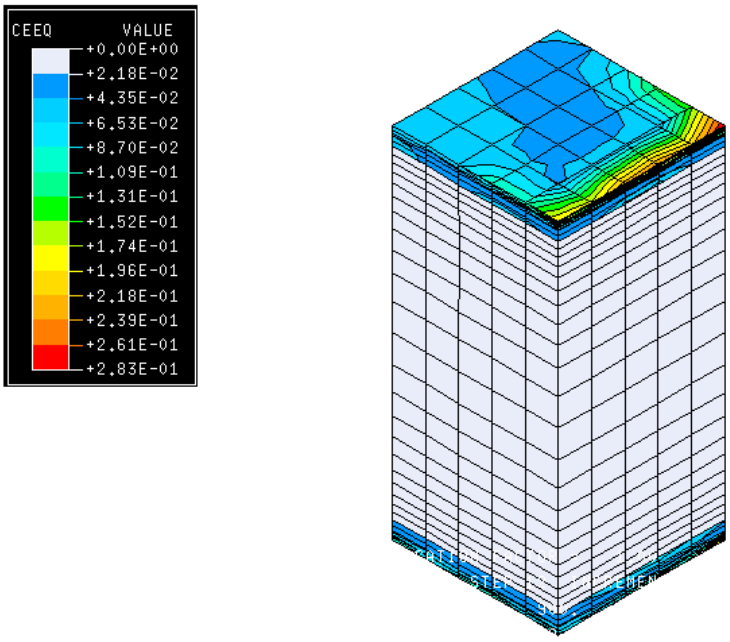

Figure IV-18 CEEQ Contour under Temperature Cycling

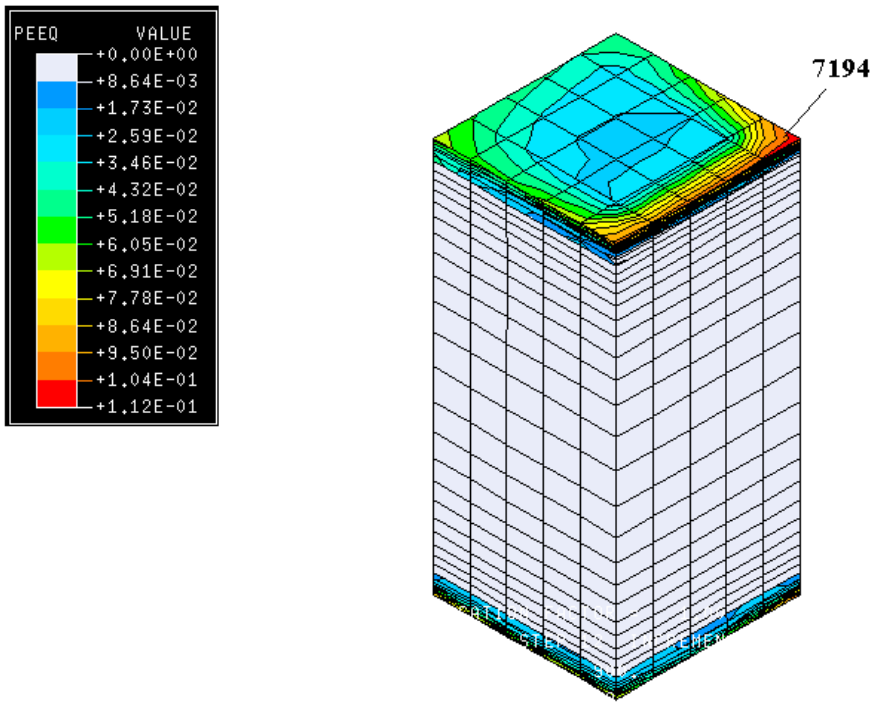

Figure IV-19 PEEQ Contour under Temperature Cycling

The stress and inelastic strain histories of element 7194 are shown in Figure IV-20 and Figure IV-21, respectively.

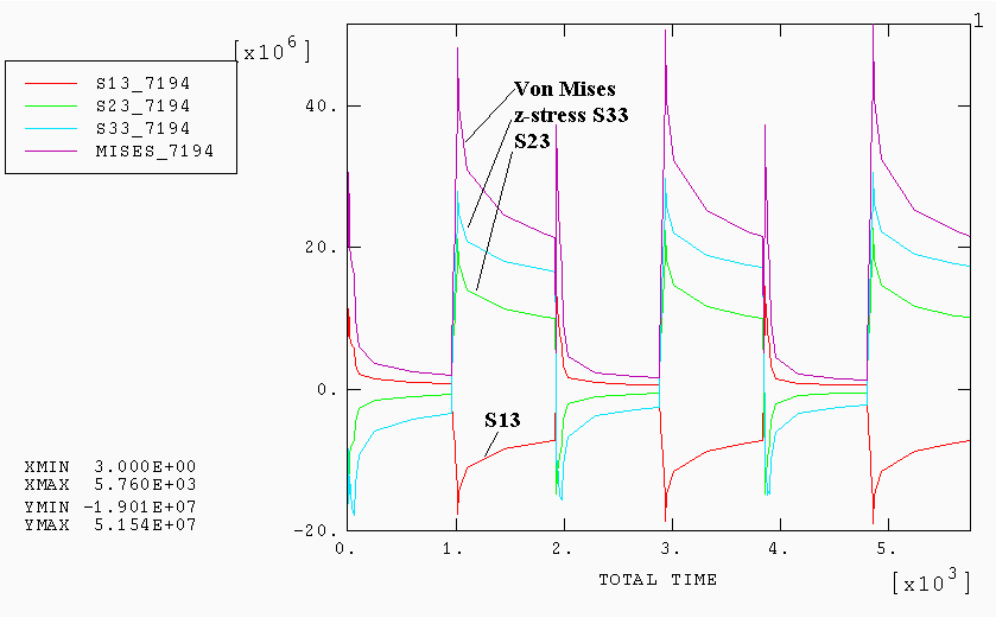

Figure IV-20 Stress History for Element 7194 under Temperature Cycling

During the initial heating stage, there is a stress peak during approximately the first 30 seconds. This is because the heating leads to increasing stresses in the solder joint. Due to the temperature-dependence of solder yield strength, it continues to decrease as the temperature increases in the range defined by the problem. When the stress level goes beyond the yield strength at a specific temperature, the solder begins to yield and this leads to the relaxation of the structure and eventual stress drop. The stress drop during the heating stage is also contributed to by the creep of solder at elevated temperature. The stress history also indicates that during heating stage, the corner of the solder joint experiences a compressive stress in the z-direction. When the structure passes the 15 minutes' holding stage and transfers to the cooling stage, the solder joint at element 7194 experiences a tensile stress of up to about 30 MPa. This is feasible since solder has a CTE of 24 ppm/K at room temperature and close to 30 ppm/K at 100°C, while the copper has a CTE of 17 ppm/K. Thus the solder deforms more than the post and DBC. In the second and third heating stage, the Von Mises stress shows a peak of about 37 MPa, which is higher than the initial stress peak. This is due to the presence of the initial stress from last cycle.

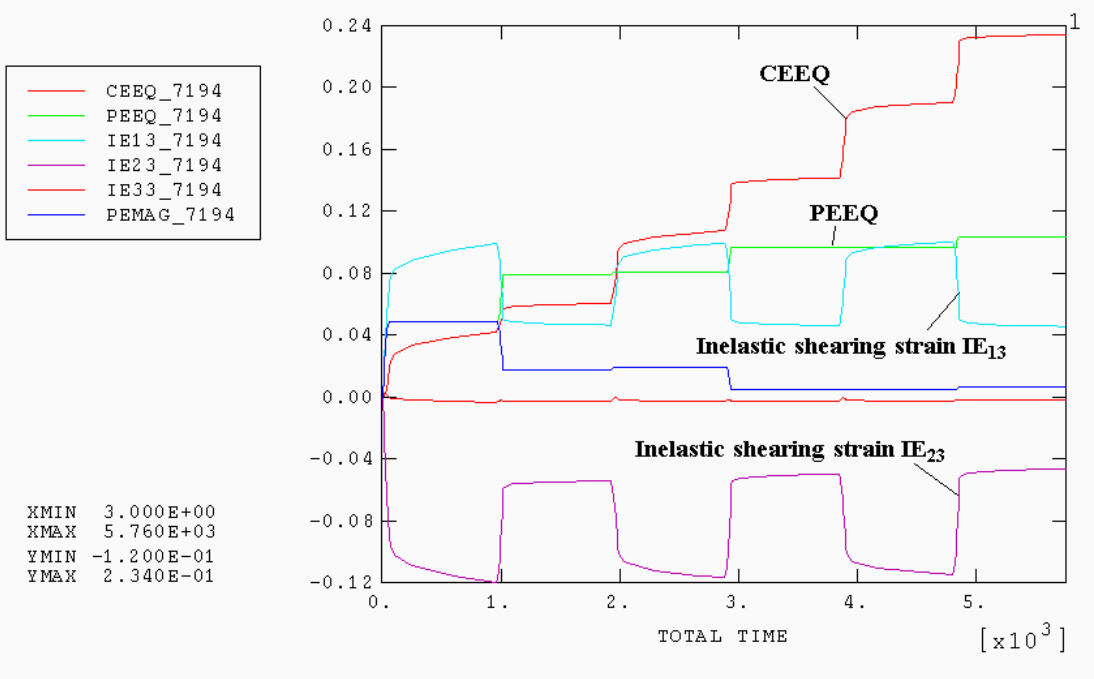

Figure IV-21 Inelastic Strain History for Element 7194 under Temperature Cycling

During the first temperature cycle, the inelastic deformation in element 7194 is controlled by plastic strain. However, at each subsequent heating and cooling stage, the accumulation rate of the CEEQ grows as that of the PEEQ decreases. Total IEEQ, however, tends to reach a saturated state after several cycles, as discussed later and shown in Figure IV-30 and Figure IV-31. The inelastic shear strain is developed on a much larger scale than the normal strain.

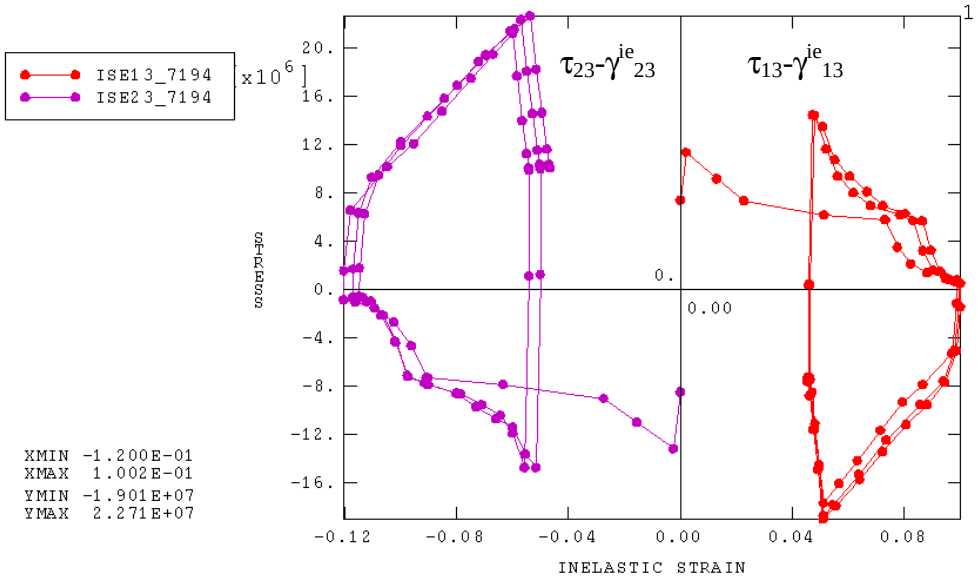

Figure IV-22 Hysteresis Loops of Shear Stress-Inelastic Shear Strain of Element 7194

Figure IV-22 shows the hysteresis loops of shear stress-inelastic shear strain curve τ_{13}-γ^{ie}_{13} and τ_{23}-γ^{ie}_{23} of element 7194. The variation of inelastic shear strain $\Delta\gamma^{ie}_{23}$ ($>\Delta\gamma^{ie}_{13}$) for each cycle has a saturated value of 0.063 after three cycles.

Figure IV-23 shows the average equivalent creep strain and equivalent plastic strain in elements 7194, 7204 and 6469 in power cycling. Figure IV-24, Figure IV-25 and Figure IV-26 show the contours of Von Mises stress, the CEEQ, and the PEEQ, respectively. Because element 6469 (located at the solder-device interface) is the weak point in power cycling, these figures show the post-to-device side of the solder joint (viewing from [1,1,-1]). After three cycles, creep deformation dominates the inelastic behavior in element 6469. This element is located at the corner of the solder where the solder meets the silicon device. It is also in the worst mechanical condition among the

three elements, with a total accumulated equivalent creep strain of 0.28. The other two locations, which are at the top of the copper post, have shown much smaller inelastic strains.

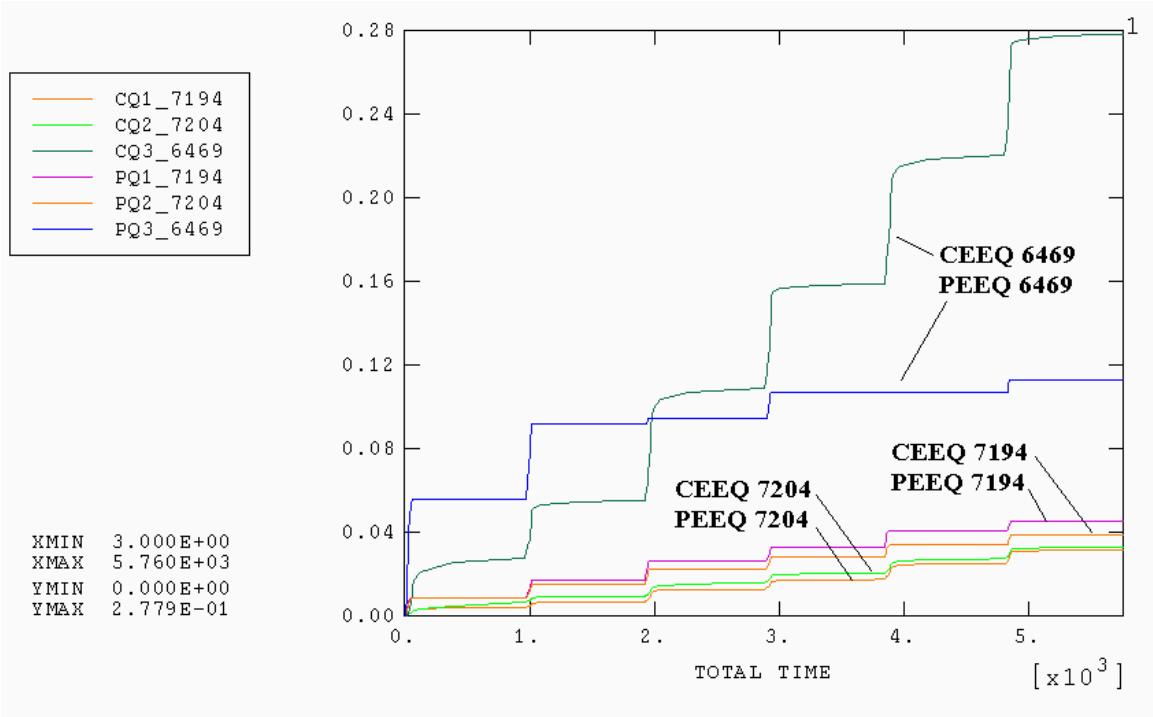

Figure IV-23 Average CEEQ and PEEQ in Element 7194, 7204 and 6469 under Power Cycling

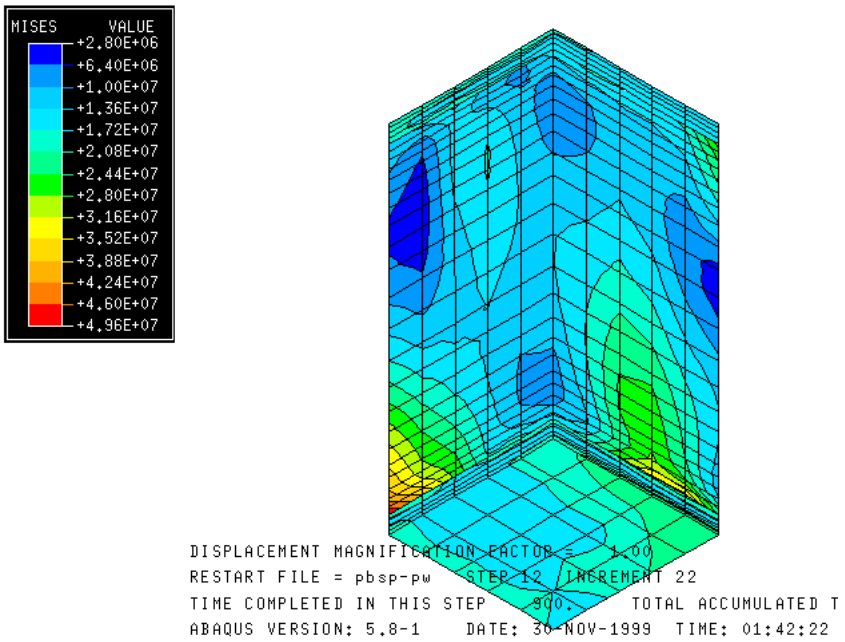

Figure IV-24 Von Mises Stress Contour under Power Cycling

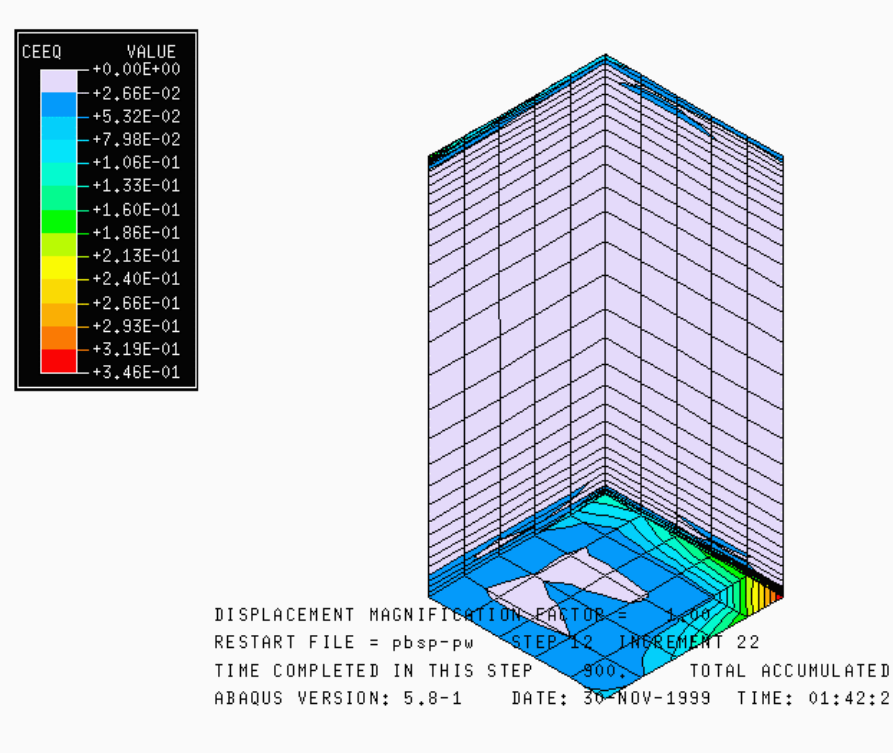

Figure IV-25 CEEQ Contour under Power Cycling

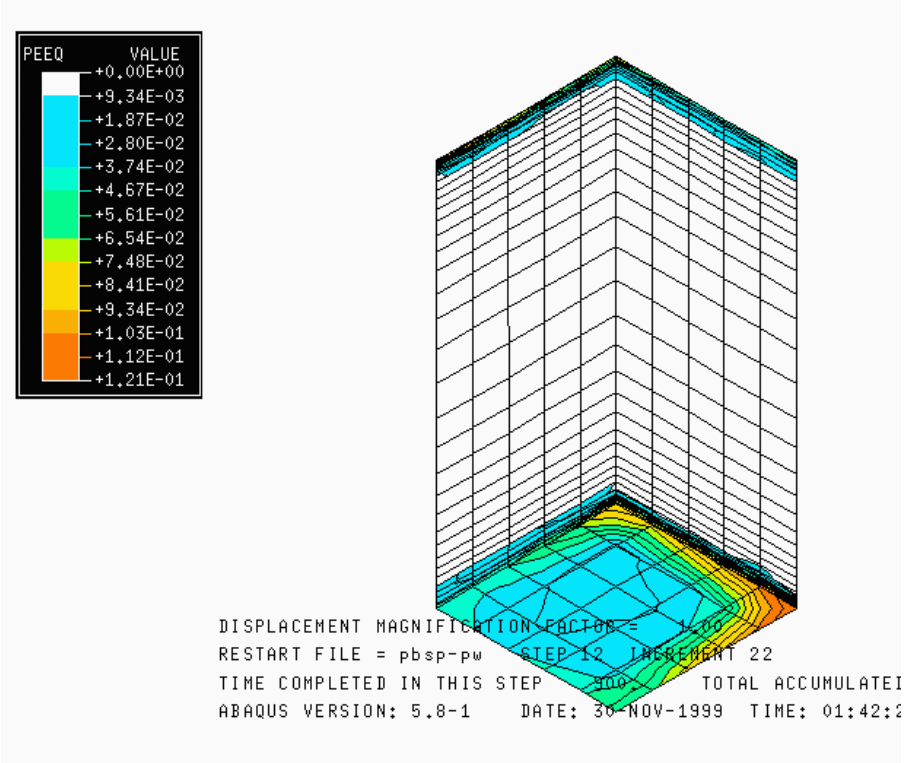

Figure IV-26 PEEQ Contour under Power Cycling

The stress and strain histories of element 6469 are shown in Figure IV-27 and Figure IV-28, respectively. Von Mises stresses show characteristics similar to those in temperature cycling. In the strain curve plot, element 6469 shows a larger accumulated creep strain than the worst-case element 7194 in temperature cycling. This is because in power cycling, the solder joints on the device side experience high temperature and high stress variation and so deform more severely than those on the top DBC side. This is also illustrated in Figure IV-23, in which the previously worst elements 7194 and 7204 (in temperature cycling) have much less CEEQ and PEEQ than those of corner element 6469 (in power cycling).

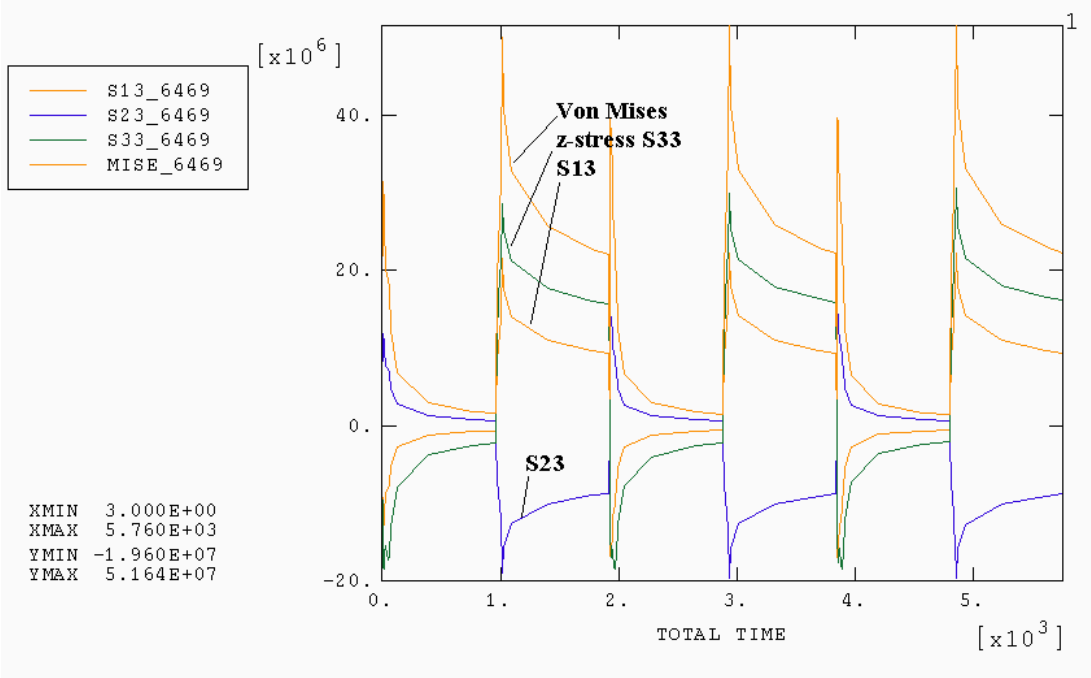

Figure IV-27 Stress History for Element 6469 under Power Cycling

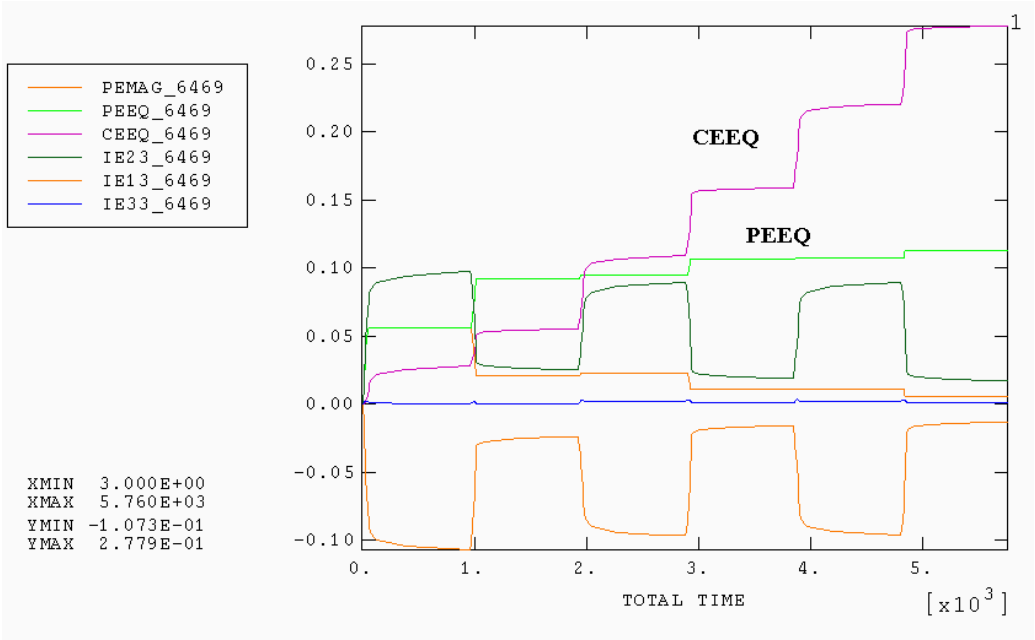

Figure IV-28 Inelastic Strain history for Element 6469 under Power Cycling

Figure IV-29 shows the hysteresis loops of the shear stress-inelastic shear strain curve τ_{13}-γ^{ie}_{13} and τ_{23}-γ^{ie}_{23} of element 6469. The variation of inelastic shear strain $\Delta\gamma^{ie}_{13}$ ($>\Delta\gamma^{ie}_{23}$) for each cycle has a saturated value of 0.078 after three cycles.

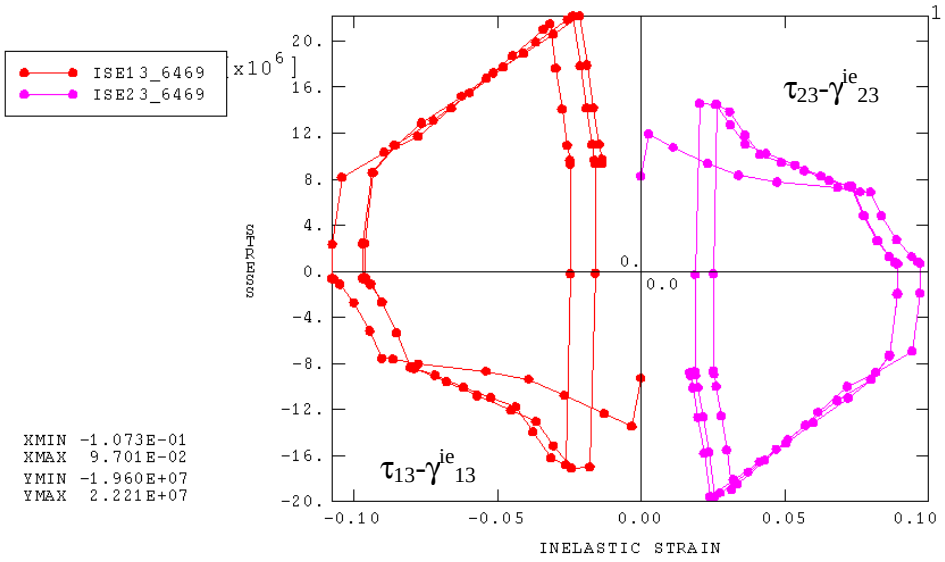

Figure IV-29 Hysteresis Loops of Shear Stress-Inelastic Shear Strain of Element 6460

4.3 Discussion

4.3.1 Fatigue Life Prediction of the Solder Joints in the MPIPPS Module

After three temperature or power cycles, the creep strain dominates the inelastic behavior and the equivalent inelastic strain accumulation rate goes into a steady state. Using a deformation-based life prediction method,[5,6] the solder joint mean fatigue life (time to 50% failure) can be estimated as:

$$N_{50} = B_1(\Delta\varepsilon_{eq}^{in})^C \tag{2}$$

where B_1 and C are material constants, and $\Delta\varepsilon_{eq}^{in}$ is the saturated IEEQ increment of the solder joint. For eutectic solder (63Sn37Pb), $B_1 = 0.146$ and $C = -1.94$.

CEEQ, PEEQ and their sum IEEQ for the three worst locations are plotted in Figure IV-30 and Figure IV-31, representing temperature cycling and power cycling conditions, respectively.

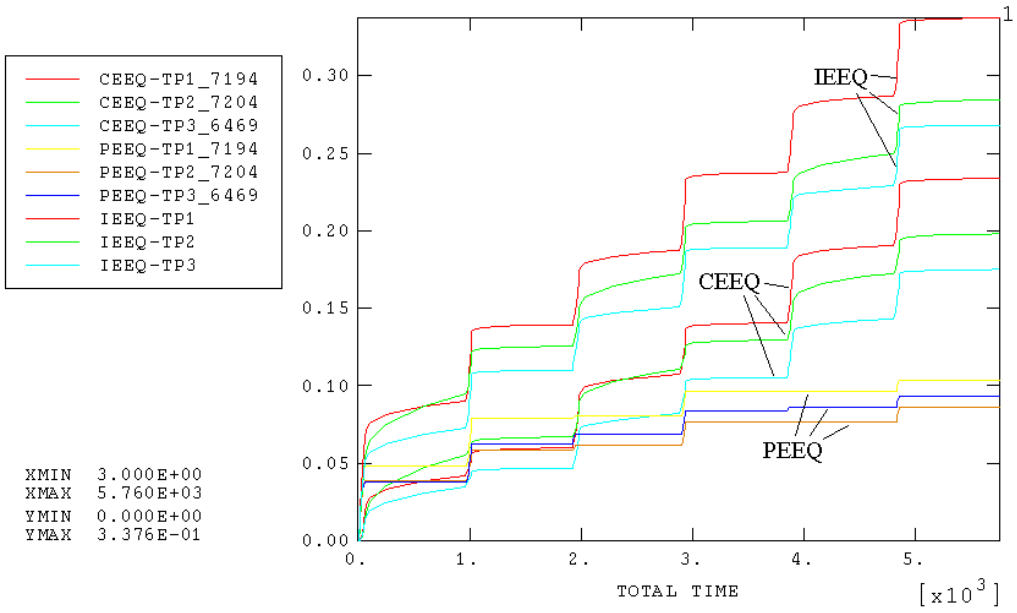

Figure IV-30 CEEQ, PEEQ and IEEQ Histories for Element 7194,7204 and 6469 under Temperature Cycling Condition

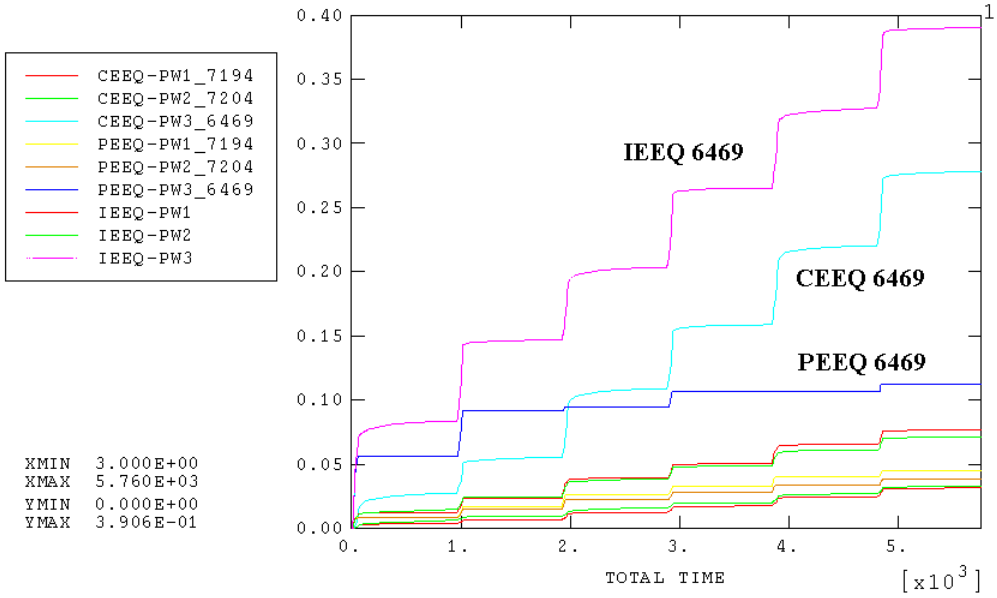

Figure IV-31 CEEQ, PEEQ and IEEQ Histories for Element 7194,7204 and 6469 under Power Cycling Condition

From the figures above we can see that in temperature cycling, the solder joint between the post and top DBC substrate deforms more than the bottom solder joint (7194 > 7204 > 6469), while the strain value are similar. Also in the power cycling condition,

the corner solder joint in between the device and the post deforms much more than the other locations. This is because in power cycling, the device-to-post solder joint experiences high temperature and stresses.

Table IV-1 lists the thermal fatigue life prediction based on FEM modeling results at the position of elements 7194, 7204 and 6469.

Table IV-1 Thermomechanical Fatigue Life Prediction

Position	$\Delta\varepsilon_{eq}^{ceep}$	$\Delta\varepsilon_{eq}^{peeq}$	$\Delta\varepsilon_{eq}^{in}$	**N_{50} (cycles)**	
				Temperature cycling	Power cycling
Elem. 7194	0.092	0.008	0.1	12.7	
	0.013	0.013	0.026		173
Elem. 7204	0.064	0.012	0.076	21.7	
	0.013	0.011	0.024		202
Elem. 6469	0.072	0.011	0.083	18.3	
	0.116	0.008	0.124		8.4

Hong's work gives an in-depth analysis of the normal fatigue life in current microelectronic technology for a 32mm CBGA package under the temperature cycling of 0^{o}C to 100^{o}C, two cycle per hour.[3] Both FEM modeling results (using the same theory for fatigue life prediction) and experiment showed a mean solder fatigue life of about 500 cycles.[3]

The 3D FEM modeling shows that the current MPIPPS module can not withstand the harsh cycling conditions used in this thesis for long. Furthermore, under power cycling conditions, the post-device solder joints are especially weak. No mature solution can be given at this point. The stacked-plate processing (MPIPPS) technique, however, does need more effort to improve its thermo-mechanical reliability by changing its overall rigid mechanical structure to a more flexible format. From a materials selection perspective, a low thermal expansion solder material with stronger resistance of high temperature creep is recommended.

4.3.2 Reliability of the Wire Bond Module

The saturated inelastic strain increment level in the wire bond module interconnect structure is of 10 to the order of one magnitude less on average than that of the MPIPPS module, as listed in Table IV-2. This is due to the very flexible interconnect structure of the wire bond module.

Table IV-2 Stresses and Inelastic Strains in the Wire Bond Model

Position	Temperature cycling		Power cycling	
	Max. Von Mises (MPa)	$\Delta\varepsilon_{eq}^{peeq}$	Max. Von Mises (MPa)	$\Delta\varepsilon_{eq}^{peeq}$
Elem. 1780	57	0.014	56.7	0.0115
Elem. 535	57	0.0118	56	0.0093
Elem. 3771	55.9	0.005	55.3	0.0005

The weak positions in the wire bond module include both the bonding interfaces. During power cycling, local heating leads to a more severe situation at the wire-device bonding interface. The location of element 1780 in the wire bond module is especially likely to fail because it developes the maximum inelastic strain. Major thermo-mechanical failure mode, according to experience, is the peeling off of emitter wire bonds. Figure IV-32 shows a sample picture taken of a burnt-out of wire bonding power module. The first wire bond disconnected from the pad due to the overshooting of the current in that wire; the subsequent increase of current to the other wires led to a small chain-reaction happened, which disconnected other wire bonds.

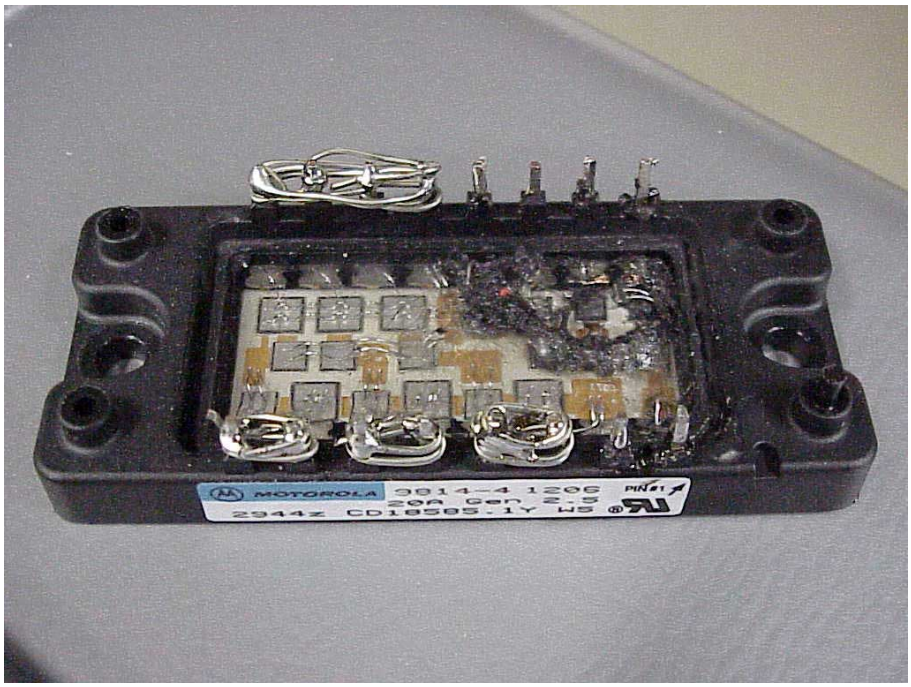

Figure IV-32 A Burnt-out Wire Bond Module Shows the Wire Debonding

I have not found any resources that estimate aluminum wire bonds' fatigue life using deformation-based theory. Most common method involves thermal cycling the wire bonding power modules. However, Vivek Mehrotra, et al has studied the reliability of wire bond based on a fracture mechanics-based model.[7] They referred to a theoretical equation,[8] which derives the driving force of debonding using the energy balance between elastic strain energy released during crack growth between wire and bonding face and the energy required to create a new crack surface area. The crack growth rate is then correlated with experimental data of Al-Al_2O_3 system and the bulk Al-Al system. There are two reasons that this method is not adopted in this thesis. First, the pure elastic model used in Vivek's work is too greatly simplified. From our modeling results the plastic deformation occurs at the interface, so using this equation could lead to erroneous estimates. And second, Vivek assumed that Al-Si exhibits the same debonding mechanism as that of the Al-Al_2O_3 system because no plastic deformation occurs in either Si and Al_2O_3. This is not exactly the case because besides stress conditions, debonding and crack growth are also closely related to the interaction at the atomic level.

Available data on commercial high power MOSFET/IGBT module reliability tests show that the first failure occurred in one of 19 tested module samples after 300 cycles (-40 to 125^{o}C temperature cycle).[9] These modules were fabricated using wire bonding technology. Compared with other emerging 3-D technology, wire bonding still dominates the power module market. One of the major reasons is that it is still the most reliable technology.

4.4 Conclusion Remarks

The thermo-mechanical responses of a wire bond module and a high power module packaged by a stacked-plate technique (MPIPPS) were studied using finite element method. Modeling results show potential weak points in both modules. The MPIPPS module raises concerns about its thermo-mechanical reliability. Improved selection of packaging materials or interconnect rearrangement to minimize thermal fatigue failure is recommended.

References

[1] Hibbitt, Karlsson and Sorensen, Inc., ABAQUS/Post Manual, Version 5.8, Pawtucket, RI, USA, 1999

[2] B. Hong and L. G. Burrell, Nonlinear Finite Element Simulation of Thermoviscoplastic Deformation of C4 Solder Joints in High Density Packaging Under Thermal Cycling, IEEE Trans. CPMT, A, Vol.8, No. 3, pp. 585-591, September 1995

[3] Bor Zen Hong, Thermal Fatigue Analysis of a CBGA Package with Lead-free Solder Fillets, InterSociety Conference on Thermal Phenomena, 205-211, Seattle, WA, USA, May 6, 1998

[4] The MacNeal-Schwendler Corporation, MSC/PATRAN Advanced FEA User's Guide, version 8, Los Angeles, CA, USA, 1999

[5] M. Mukai, T. Kawakami, K. Takahashi and N. Iwase, Thermal Fatigue Life Prediction of Solder Joints using Stress Analysis, International Electronic Manufacturing Technology Symposium, pp. 204-208, Omiya, Japan, April 1997

[6] Bor Zen Hong and Tsorng-Dih Yuan, Integrated Flow-Thermomechanical and Reliability Analysis of a Densely Packed C4/CBGA Assembly, InterSociety Conference on Thermal Phenomena, pp. 220-228, Seattle, WA, USA, May 6, 1998

[7] Vivek Mehrotra, Jun He, Mahyar S. Dadkhah, Kevin Rugg and Michael C. Shaw, Wirebond Reliability in IGBT-Power Modules: Application of High Resolution Strain and Temperature Mapping, IEEE ISPSD'99, Proceedings of the 11th International Symposium on Power Semiconductor Devices and ICs, pp. 113-116, Toronto, Ontario, Canada, May 26-28, 1999

[8] H. Tada, P. C. Paris and G. R. Irwin, The Stress Analysis of Cracks Handbook, Second Edition, Paris Production Inc., St. Louis, MO, USA 1985

[9] IXYS, Power Semiconductor Devices Reliability Report, July 1997-June 1999, IXYS Corporation, Santa Clara, CA, USA, September 1999